Engineering with Computers (2022) 38:3691–3704
https://doi.org/10.1007/s00366-021-01390-y

ORIGINAL ARTICLE

# Quasi-3D large deflection nonlinear analysis of isogeometric FGM microplates with variable thickness via nonlocal stress–strain gradient elasticity

**Xiaoxia Ma**[1] · **Saeid Sahmani**[2] · **Babak Safaei**[3]

Received: 14 February 2021 / Accepted: 19 March 2021 / Published online: 29 April 2021


**Abstract**

Via the nonlocal stress–strain gradient continuum mechanics, the microscale-dependent linear and nonlinear large deflections of transversely loaded composite sector microplates with different thickness variation schemes are investigated. Microplates are assumed to be prepared from functionally graded materials (FGMs) the characteristics of which are changed along the thickness direction. A quasi-3D plate theory with a sinusoidal transverse shear function in conjunction with a trigonometric normal function was employed for the establishment of size-dependent modelling of FGM microplates with different thickness variation schemes. Then, to solve the nonlocal stress–strain gradient flexural problem, the non-uniform rational B-spline type of isogeometric solution methodology was applied for an accurate integration of geometric discerptions. It was found that the gap between load–deflection curves drawn for linear, concave and convex thickness variation patterns became greater by changing FGM composite microplate boundary conditions from clamped to simply supported. In addition, it was found that by considering only the nonlocal size effect, the plate deflection obtained by the nonlocal strain gradient quasi-3D plate model was greater than that extracted by the classical continuum elasticity because of the softening character of nonlocal size effect, while the strain gradient microstructural size dependency acted in opposite way and represented a stiffening character.

**Keywords** Nonlocal stress effect · Nonlinear flexural response · Normal shape function · Thickness variation · Elliptical plates

## 1 Introduction

As an emerging and modern and inhomogeneous material class, functionally graded materials (FGMs) meet several requirements of engineering applications including effective stress control leading the creation of several application areas for these materials. Kumar et al. [1] developed polymer–ceramic continuous quartz fiber reinforced FGM composites to be applied in thermos-structural aerospace applications. Qin and his colleagues investigated wave propagation behavior of FGM porous plates reinforced with graphene platelets [2] and conducted analytical study on impact response of sandwich cylindrical shell with a FGM porous core [3]. Besides, they have carried out a series of studies on vibrations of FGM plates and shells with non-classic boundary conditions [4–6], which benefits the application of plates and shells in engineering fields. On the other hand, advanced composite materials have widely utilized for several applications such as dynamic sensors [7], reinforced beam structures [8–12], lithium–ion battery [13], digital microscopes [14, 15], and dampers [16].

In the past decade, new fabrication processes have been proposed incorporating FGM composite concept in micro-electro-mechanical structures and systems. In this regard, it of great importance to take various size dependency features in mechanical properties of microstructures made of FGM composite. For example, Jung and Han [17] studied Sigmoid FGM composite microplate mechanical behaviors based on modified couple stress elasticity. Li and Pan [18]

✉ Xiaoxia Ma
XiaoxiaMa@21cn.com

1 Department of Basic Courses, Jiaozuo University, Jiaozuo 454000, China

2 Mechanical Rotating Equipment Department, Niroo Research Institute (NRI), 14665-517 Tehran, Iran

3 Department of Mechanical Engineering, Eastern Mediterranean University, Famagusta, North Cyprus via Mersin 10, Turkey

predicted FGM piezoelectric microplate static bending when symmetric couple stress tensor was present. Simsek [19] developed a nonlocal strain gradient Euler–Bernoulli beam model for nonlinear vibration behaviors of FGM composite nanobeam structures according to a novel Hamiltonian method. Sahmani and Aghdam [20] applied surface elasticity theory to investigate imperfection sensitivity of postbuckling behaviors of pressurized FGM composite cylindrical nanoshells. Liu et al. [21] investigated biaxial buckling and nonlocal oscillations properties of double viscoelastic FGM composite nanoplates under in-plane edge loads. Sahmani and Aghdam [22–24] determined critical buckling loads and postbuckling equilibrium paths of hybrid FGM composite cylindrical nanoshells based on nonlocal continuum theory. Phung-Van et al. [25] developed a generalized shear deformation plate theory for nonlinear transient response of piezoelectric FGM plates subjected to thermos-electro-mechanical loads using isogeometric technique. Nguyen et al. [26] employed a refined quasi-3D plate model incorporating couple stress size for FM composite microplates. Van et al. [27] derived a suitable computational equation for size-dependent nonlinear transient behaviors of FGM composite nanoplates based on isogeometric analysis. Chu et al. [28] predicted flexoelectric effect on FGM piezoelectric microbeam bending behaviors based on general modified strain gradient elasticity.

Recently, Khakalo et al. [29] modeled size-dependent 2D triangular lattices on the basis of strain gradient model for the analysis of mechanical responses of auxetics and sandwich beams. She et al. [30] studied the oscillations and nonlinear bending of FGM porous microtubes based on nonlocal strain gradient elasticity. Pang et al. [31] analytically explored viscoelastic nanoplate transverse oscillations using simply supported boundary conditions including high-order surface stress size effect. Sahmani et al. [32–35] predicted the nonlinear vibration and bending properties of graphene platelet-reinforced FGM porous third-order shear deformable microbeams based on nonlocal strain gradient continuum mechanics. Phung-Van et al. [36] investigated numerically the porosity-dependent nonlinear transient characteristics of FGM nanoplates with the aid of isogeometric method. Li et al. [37] used modified strain gradient theory of elasticity for the analysis of vibrations and static bending of organic solar cells surrounded by Winkler–Pasternak elastic foundation. Thanh et al. [38] established a modified couple stress-based Reddy plate model for the simulation of composite laminated microplate thermal bending behaviors. Sahmani and Safaei [39–41] analyzed size-dependent nonlinear mechanical responses of bi-directional FGM microbeams. Fan et al. [42–44] anticipated FGM porous microplate size-dependent responses according to various non-classical continuum theories. Ghorbani et al. [45] combined Gurtin–Murdoch and nonlocal strain gradient theories of elasticity to derive cylindrical microshell size-dependent natural frequencies. Yuan et al. [46–48] established size-dependent conical shell models to evaluate FGM composite conical microshell nonlinear mechanical properties. Ghobadi et al. [49] developed a continuous size-dependent electro-mechanical model for the analysis nonlinear thermos-electro-mechanical vibration behaviors of FGM flexoelectric nanoplate structures. Thai et al. [50] proposed a nonlocal meshfree model for the determination of size-dependent frequencies and deformations of FGM carbon nanotube-reinforced nanoplates. Yuan et al. [51] investigated shear buckling behaviors of FGM composite skew nanoplates under surface residual stress and surface elasticity. Yi et al. [52], and Li et al. [53] took into account the interactions among vibration modes for the analysis of surface elastic-based large-amplitude free vibrations of porous FGM composite nanoplates. Fan et al. [54] analyzed the couple stress effect on the dynamic stability of FGM conical microshells having magnetostrictive facesheets surrounded by a viscoelastic foundation. Sarafraz et al. [55], and Xie et al. [56] established a surface elastic beam model to predict the nonlinear secondary resonance of FGM porous nanobeams under periodic excitation. Yang et al. [57] employed a perturbation-based solving process for postbuckling analysis of hydrostatic pressurized nonlocal strain gradient FGM microshells.

The aim of this research was to develop nonlocal strain gradient quasi-3D nonlinear flexural solving process for FGM microplates with various thickness variation patterns. Therefore, a quasi-3D plate model based on nonlocal strain gradient continuum mechanics with sinusoidal transverse shear and trigonometric normal functions were employed. Then, the proposed refined quasi-3D nonlocal strain gradient plate model was combined with isogeometric technique incorporating geometric description and finite element approximation for accurately solving nonlinear problems for different thickness variation patterns.

## 2 Nonlocal strain gradient quasi-3D FGM variable thickness plate model

Here, as shown in Fig. 1, two sector and elliptical shapes have been taken into account for FGM composite microplates with variable thickness $h(x, y)$. For elliptical shape, $a$ and $b$ denote long and short axes, respectively. For sector microplates, $\alpha$ and $r_0$ represent angle and radius, respectively.

For estimating effective material characteristics of Poisson's ratio $\nu(z)$ and Young's modulus $E(z)$ of FGM composite microplates, Mori–Tanaka scheme homogenization scheme were considered. Therefore, effective bulk and shear moduli were determined according to homogenization model as:

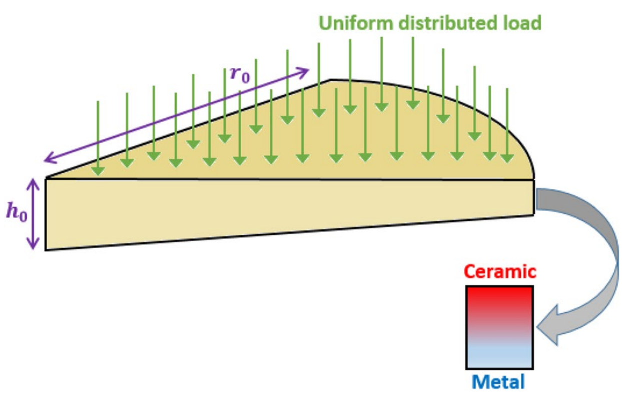


**Fig. 1** Schematic representation of a FGM sector microplate with variable thickness under uniform distributed load

$$K(z) = K_m + \frac{\left(\frac{1}{2}+\frac{z}{h}\right)^k}{\frac{1}{K_c-K_m} + \frac{3\left[1-\left(\frac{1}{2}+\frac{z}{h}\right)^k\right]}{3K_m+4G_m}}, \tag{1a}$$

$$G(z) = G_m + \frac{\left(\frac{1}{2}+\frac{z}{h}\right)^k}{\frac{1}{G_c-G_m} + \frac{6(K_m+2G_m)\left[1-\left(\frac{1}{2}+\frac{z}{h}\right)^k\right]}{5G_m(3K_m+4G_m)}}, \tag{1b}$$

where $k$ is material property gradient index and

$$K_m = \frac{E_m}{3(1-2\nu_m)}, K_c = \frac{E_c}{3(1-2\nu_c)},$$
$$G_m = \frac{E_m}{2(1+\nu_m)}, G_c = \frac{E_c}{2(1+\nu_c)}. \tag{2}$$

Also, subscripts $c$ and $m$ denote ceramic and metal phases of FGM composite microplates, respectively.

To determine microplate thickness variations for sector and elliptical shapes, the following functions were considered for a sector microplates:

$$h(x,y) = h_0\left[1-\frac{1}{2}\left(\frac{\sqrt{x^2+y^2}}{r_0}\right)^\eta\right], \tag{3}$$

where $\eta$ and $h_0$ are thickness variation constant showing variable thickness type and maximum plate thickness, respectively. Therefore, concave, linear, and convex thickness variation types are related to $\eta > 1, \eta = 1$ and $\eta < 1$, respectively.

Figures 2 and 3 compare linear thickness variations with convex and concave ones, respectively, for various thickness variation constants.

The quasi-3D modelling of a microplate was stated as follows by taking into account normal strains using a transverse normal shape function $\mathbb{g}(z)$ and dividing transverse displacement component into shear bending and variables:

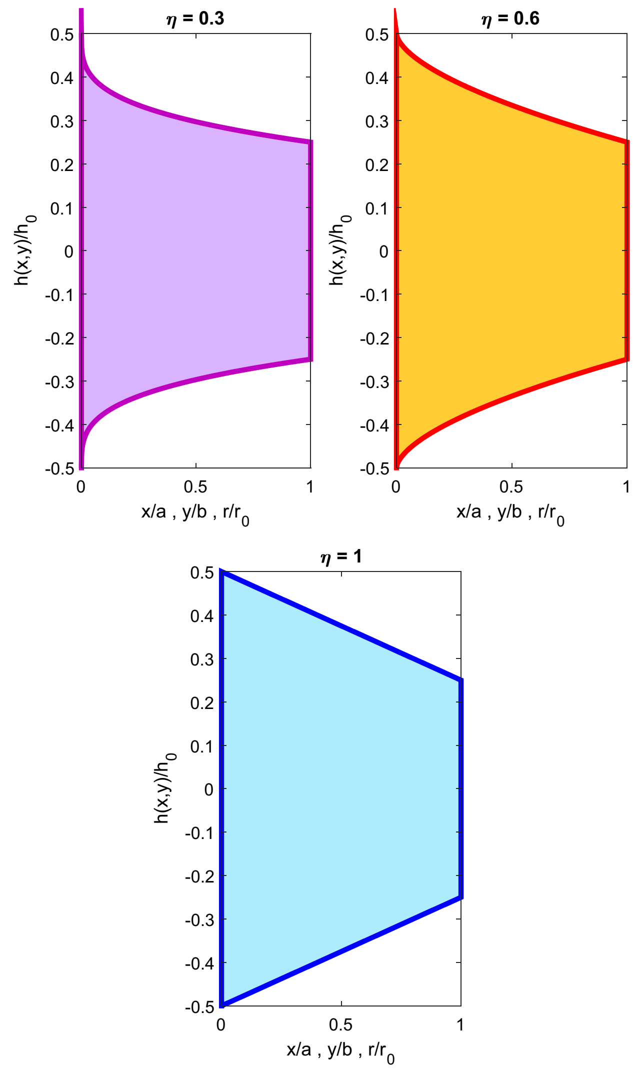


**Fig. 2** Illustration of convex and linear variations of the plate thickness for sector microplates corresponding to different thickness variation constants

$$\mathcal{U}_x(x,y,z) = u(x,y) - zw_{b,x}(x,y) + \mathbb{F}(z)w_{s,x}(x,y), \tag{4a}$$

$$\mathcal{U}_y(x,y,z) = v(x,y) - zw_{b,y}(x,y) + \mathbb{F}(z)w_{s,y}(x,y), \tag{4b}$$

$$\mathcal{U}_z(x,y,z) = w_b(x,y) + \mathbb{G}(z)w_s(x,y), \tag{4c}$$

where $w_s(x,y)$ and $w_b(x,y)$ are shear and bending displacement variables according to hybrid quasi-3D-based higher order shear deformation plate model. By assuming normal shape and transverse shear functions as sinusoidal trigonometric ones, it was found that

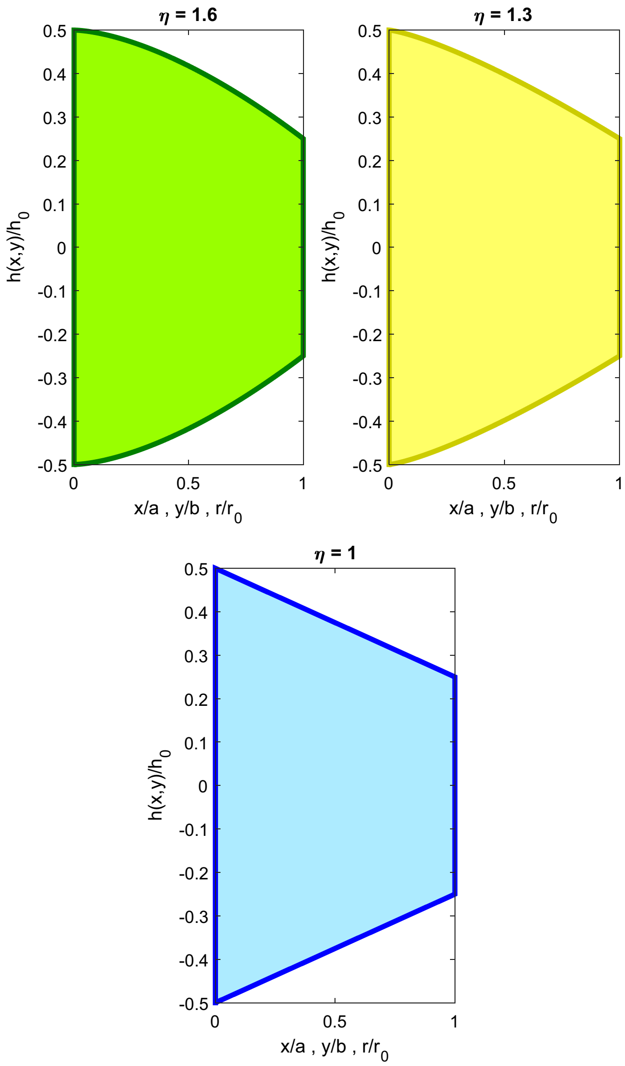


**Fig. 3** Illustration of concave and linear variations of the plate thickness for sector microplates corresponding to different thickness variation constants

$$\mathbb{F}(z) = \sin(\pi z/h) - z, \tag{5a}$$

$$\mathbb{G}(z) = 1 + (5/12\pi)\cos(\pi z/h). \tag{5b}$$

Considering von-Karman nonlinear kinematics including large deflections and moderate rotations, the associated hybrid quasi-3D-based strain components were stated as:

$$\begin{aligned}
\varepsilon_{xx} &= u_{,x} + \frac{\left(w_{b,x} + w_{s,x}\right)^2}{2} - zw_{b,xx} + \mathbb{F}(z)w_{s,xx},\\
\varepsilon_{yy} &= v_{,y} + \frac{\left(w_{b,y} + w_{s,y}\right)^2}{2} - zw_{b,yy} + \mathbb{F}(z)w_{s,yy},\\
\varepsilon_{zz} &= \mathbb{G}_{,z}(z)w_s,\\
\gamma_{xy} &= u_{,y} + v_{,x} + \left(w_{b,x} + w_{s,x}\right)\left(w_{b,y} + w_{s,y}\right) - 2zw_{b,xy} + 2\mathbb{F}(z)w_{s,xy},\\
\gamma_{xz} &= \left(\mathbb{F}_{,z}(z) + \mathbb{G}(z)\right)w_{s,x},\\
\gamma_{yz} &= \left(\mathbb{F}_{,z}(z) + \mathbb{G}(z)\right)w_{s,y}.
\end{aligned} \tag{6}$$

Consequently, stress–strain constitutive relationships were written as:

$$\begin{aligned}
\sigma_{xx} &= \frac{E(z)}{(1+\nu(z))(1-2\nu(z))}\varepsilon_{xx} + \frac{\nu(z)E(z)}{(1+\nu(z))(1-2\nu(z))}\left(\varepsilon_{yy} + \varepsilon_{zz}\right),\\
\sigma_{yy} &= \frac{E(z)}{(1+\nu(z))(1-2\nu(z))}\varepsilon_{yy} + \frac{\nu(z)E(z)}{(1+\nu(z))(1-2\nu(z))}\left(\varepsilon_{xx} + \varepsilon_{zz}\right),\\
\sigma_{zz} &= \frac{E(z)}{(1+\nu(z))(1-2\nu(z))}\varepsilon_{zz} + \frac{\nu(z)E(z)}{(1+\nu(z))(1-2\nu(z))}\left(\varepsilon_{xx} + \varepsilon_{yy}\right),\\
\tau_{xy} &= \frac{E(z)}{2(1+\nu(z))}\gamma_{xy},\ \tau_{yz} = \frac{E(z)}{2(1+\nu(z))}\gamma_{yz},\ \tau_{xz} = \frac{E(z)}{2(1+\nu(z))}\gamma_{xz}.
\end{aligned} \tag{7}$$

By employing nonlocal strain gradient continuum elasticity, total stress tensor was stated as [58]:

$$\Phi_{ij} = \sigma_{ij} - \nabla\sigma^*_{ijm}, \tag{8}$$

where classical and higher order stresses, respectively, were described:

$$\sigma_{ij} = \int_V \chi_1\left(x', x, e_1\right)C_{ijkl}\varepsilon_{kl}dV, \tag{9a}$$

$$\sigma^*_{ijm} = l^2\int_V \chi_2\left(x', x, e_2\right)C_{ijkl}\varepsilon_{kl,m}dV, \tag{9b}$$

where $e_1$ and $e_2$ represent nonlocal parameters corresponding to size dependency due to nonlocal stress. Also, $l$ is length scale parameter incorporating strain gradient size effect. $C_{ijkl}$, $\varepsilon_{kl}$, and $\varepsilon_{kl,m}$ are elastic coefficients, strain components, and strain gradient components, respectively. Based on nonlocal strain gradient theory, it was assumed that $\chi_1\left(x', x, e_1\right)$

and $\chi_2(x', x, e_2)$ two kernel functions had to equilibrate the conditions introduced by Eringen [59] as:

$$\sigma_{ij} - e_1^2(\sigma_{ij,xx} + \sigma_{ij,yy}) = C_{ijkl}\varepsilon_{kl}, \tag{10a}$$

$$\sigma^*_{ijm} - e_2^2\left(\sigma^*_{ijm,xx} + \sigma^*_{ijm,yy}\right) = l^2 C_{ijkl}\varepsilon_{kl,m}. \tag{10b}$$

Therefore, generalized constitutive equation based on nonlocal strain gradient elasticity was stated as:

$$\begin{aligned}&\left[1 - e_1^2(_{,xx} + _{,yy})\right]\left[1 - e_2^2(_{,xx} + _{,yy})\right]\Phi_{ij} = \left[1 - e_1^2(_{,xx} + _{,yy})\right] \\ &\quad C_{ijkl}\varepsilon_{kl} - l^2\left[1 - e_2^2(_{,xx} + _{,yy})\right]C_{ijkl}\left(\varepsilon_{kl,xx} + \varepsilon_{kl,yy}\right).\end{aligned} \tag{11}$$

Assuming $e_1 = e_2 = e$, it was found that

$$\Phi_{ij} - e^2\left(\Phi_{ij,xx} + \Phi_{ij,yy}\right) = C_{ijkl}\varepsilon_{kl} - l^2 C_{ijkl}\left(\varepsilon_{kl,xx} + \varepsilon_{kl,yy}\right). \tag{12}$$

Therefore, strain energy variations for quasi-3D nonlocal strain gradient FGM microplates with various shapes and thicknesses were written as:

$$\delta\Pi_S = \int_S \int_{-\frac{h(x,y)}{2}}^{\frac{h(x,y)}{2}} \Phi_{ij}\delta\varepsilon_{ij}\,dz\,dS. \tag{13}$$

In addition, the induced virtual work by external distributed load $q$ was stated as:

$$\delta\Pi_W = \int_S q\delta w dS. \tag{14}$$

Virtual work principle was employed along with the substitution of Eqs. (6) and (7) into Eq. (13) resulting in

$$\begin{aligned}&\int_S \{\delta(\mathfrak{P}_b^T)\xi_b\mathfrak{P}_b - l^2\delta(\nabla^2\mathfrak{P}_b^T)\xi_b\mathfrak{P}_b + \delta(\mathfrak{P}_s^T)\xi_s\mathfrak{P}_s \\ &-l^2\delta(\nabla^2\mathfrak{P}_s^T)\xi_s\mathfrak{P}_s\}dS = \int_S (1 - e^2\nabla^2)\amalg\delta w dS,\end{aligned} \tag{15}$$

where

$$\mathfrak{P}_b = \begin{bmatrix} u_{,x} + (w_{b,x} + w_{s,x})^2/2 & -w_{b,xx} & w_{s,xx} & 0 \\ v_{,y} + (w_{b,y} + w_{s,y})^2/2 & -w_{b,yy} & w_{s,yy} & 0 \\ u_{,y} + v_{,x} + (w_{b,x} + w_{s,x})(w_{b,y} + w_{s,y}) & -2w_{b,xy} & 2w_{s,xy} & 0 \\ 0 & 0 & 0 & w_s \end{bmatrix}^T,$$

$$\xi_b = \begin{bmatrix} \mathbf{A_b} & \mathbf{B_b} & \mathbf{C_b} & \mathbf{E_b} \\ \mathbf{B_b} & \mathbf{D_b} & \mathbf{F_b} & \mathbf{G_b} \\ \mathbf{C_b} & \mathbf{F_b} & \mathbf{H_b} & \mathbf{K_b} \\ \mathbf{E_b} & \mathbf{G_b} & \mathbf{K_b} & \mathbf{J_b} \end{bmatrix}, \mathfrak{P}_s = \begin{bmatrix} w_{s,x} \\ w_{s,y} \end{bmatrix}, \tag{16}$$

$$\xi_s = \int_{-\frac{h(x,y)}{2}}^{\frac{h(x,y)}{2}} \left(\mathbb{F}_{,z}(z) + \mathbb{G}(z)\right)^2 \begin{bmatrix} Q_{44}(z) & 0 \\ 0 & Q_{55}(z) \end{bmatrix} dz,$$

where stress-based stiffness parameters was defined as:

$$\begin{aligned}
\{\mathbf{A_b}, \mathbf{B_b}, \mathbf{C_b}\} &= \int_{-\frac{h(x,y)}{2}}^{\frac{h(x,y)}{2}} \begin{bmatrix} \frac{1}{1-2\nu(z)} & \frac{\nu(z)}{1-2\nu(z)} & 0 & \frac{\nu(z)}{1-2\nu(z)} \\ \frac{\nu(z)}{1-2\nu(z)} & \frac{1}{1-2\nu(z)} & 0 & \frac{\nu(z)}{1-2\nu(z)} \\ 0 & 0 & 1/2 & 0 \\ \frac{\nu(z)}{1-2\nu(z)} & \frac{\nu(z)}{1-2\nu(z)} & 0 & \frac{1}{1-2\nu(z)} \end{bmatrix} \frac{E(z)}{1+\nu(z)}\{1, z, \mathbb{F}(z)\}dz, \\
\{\mathbf{D_b}, \mathbf{E_b}\} &= \int_{-\frac{h(x,y)}{2}}^{\frac{h(x,y)}{2}} \begin{bmatrix} \frac{1}{1-2\nu(z)} & \frac{\nu(z)}{1-2\nu(z)} & 0 & \frac{\nu(z)}{1-2\nu(z)} \\ \frac{\nu(z)}{1-2\nu(z)} & \frac{1}{1-2\nu(z)} & 0 & \frac{\nu(z)}{1-2\nu(z)} \\ 0 & 0 & 1/2 & 0 \\ \frac{\nu(z)}{1-2\nu(z)} & \frac{\nu(z)}{1-2\nu(z)} & 0 & \frac{1}{1-2\nu(z)} \end{bmatrix} \frac{E(z)}{1+\nu(z)}\left\{z^2, \mathbb{G}_{,z}(z)\right\}dz, \\
\{\mathbf{F_b}, \mathbf{G_b}, \mathbf{H_b}\} &= \int_{-\frac{h(x,y)}{2}}^{\frac{h(x,y)}{2}} \begin{bmatrix} \frac{1}{1-\nu 2(z)} & \frac{\nu(z)}{1-2\nu(z)} & 0 & \frac{\nu(z)}{1-2\nu(z)} \\ \frac{\nu(z)}{1-2\nu(z)} & \frac{1}{1-2\nu(z)} & 0 & \frac{\nu(z)}{1-2\nu(z)} \\ 0 & 0 & 1/2 & 0 \\ \frac{\nu(z)}{1-2\nu(z)} & \frac{\nu(z)}{1-2\nu(z)} & 0 & \frac{1}{1-2\nu(z)} \end{bmatrix} \frac{E(z)}{1+\nu(z)}\left\{z\mathbb{F}(z), z\mathbb{G}_{,z}(z), \mathbb{F}^2(z)\right\}dz, \\
\{\mathbf{K_b}, \mathbf{J}_b\} &= \int_{-\frac{h(x,y)}{2}}^{\frac{h(x,y)}{2}} \begin{bmatrix} \frac{1}{1-2\nu(z)} & \frac{\nu(z)}{1-2\nu(z)} & 0 & \frac{\nu(z)}{1-2\nu(z)} \\ \frac{\nu(z)}{1-2\nu(z)} & \frac{1}{1-2\nu(z)} & 0 & \frac{\nu(z)}{1-2\nu(z)} \\ 0 & 0 & 1/2 & 0 \\ \frac{\nu(z)}{1-2\nu(z)} & \frac{\nu(z)}{1-2\nu(z)} & 0 & \frac{1}{1-2\nu(z)} \end{bmatrix} \frac{E(z)}{1+\nu(z)}\left\{\mathbb{F}(z)\mathbb{G}_{,z}(z), \left(\mathbb{G}_{,z}(z)\right)^2\right\}dz.
\end{aligned} \tag{17}$$

## 3 Isogeometric finite element framework

Isogeometric technique is a new solution method for connecting finite element and computer aided design approaches to determine geometrical description and an efficient numerical approximation [60–68]. The considered cubic elements for a sector microplate is depicted in Fig. 4.

Considering rational functions of B-splines, displacement field in a plate-type domain satisfying C$^{-1}$-requirement essential for the developed quasi-3D plate model was approximated as:

$$\left\{ \tilde{u}^i, \tilde{v}^i, \tilde{w}_b^i, \tilde{w}_s^i \right\}^T = \sum_{i=1}^{m\times n} G_i(x,y) \begin{Bmatrix} u^i \\ v^i \\ w_b^i \\ w_s^i \end{Bmatrix}, \tag{18}$$

where

$$G_i(x,y) = \begin{bmatrix} \mathfrak{X}_i(x,y) & 0 & 0 & 0 \\ 0 & \mathfrak{X}_i(x,y) & 0 & 0 \\ 0 & 0 & \mathfrak{X}_i(x,y) & 0 \\ 0 & 0 & 0 & \mathfrak{X}_i(x,y) \end{bmatrix}. \tag{19}$$

According to Eqs. (18) and (19), strain components were rewritten as:

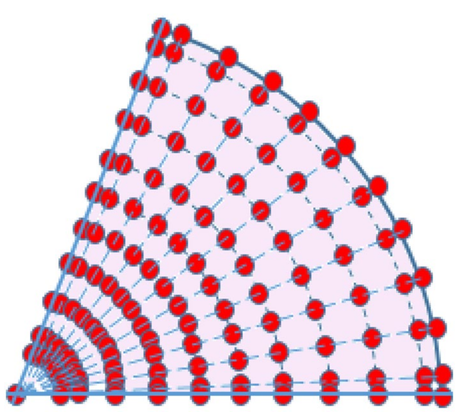

**Fig. 4** Representation of cubic elements for a sector microplate

$$\mathfrak{F}_b = \mathfrak{F}_b^L + \mathfrak{F}_b^{NL} = \sum_{i=1}^{m\times n} \Upsilon_{Lb}^i \mathbb{X} + \sum_{i=1}^{m\times n} \frac{1}{2} \Upsilon_{NLb}^i \mathbb{X}, \mathfrak{F}_s = \sum_{i=1}^{m\times n} \Upsilon_s^i \mathbb{X}, \tag{20}$$

where

$$\Upsilon_{Lb}^i = \left\{ \Upsilon_{b1}^i \; \Upsilon_{b2}^i \; \Upsilon_{b3}^i \; \Upsilon_{b4}^i \right\}^T, \Upsilon_{NLb}^i = \left\{ \Upsilon_{b5}^i \; 0 \; 0 \; 0 \right\}^T \Upsilon_G^i, \mathbb{X} = \begin{Bmatrix} u^i \\ v^i \\ w_b^i \\ w_s^i \end{Bmatrix},$$

$$\Upsilon_{b1}^i = \begin{bmatrix} \mathfrak{X}_{i,x}(x,y) & 0 & 0 & 0 \\ 0 & \mathfrak{X}_{i,y}(x,y) & 0 & 0 \\ \mathfrak{X}_{i,y}(x,y) & \mathfrak{X}_{i,x}(x,y) & 0 & 0 \\ 0 & 0 & 0 & 0 \end{bmatrix}, \Upsilon_{b2}^i = -\begin{bmatrix} 0 & 0 & \mathfrak{X}_{i,xx}(x,y) & 0 \\ 0 & 0 & \mathfrak{X}_{i,yy}(x,y) & 0 \\ 0 & 0 & 2\mathfrak{X}_{i,xy}(x,y) & 0 \\ 0 & 0 & 0 & 0 \end{bmatrix},$$

$$\Upsilon_{b3}^i = \begin{bmatrix} 0 & 0 & 0 & \mathfrak{X}_{i,xx}(x,y) \\ 0 & 0 & 0 & \mathfrak{X}_{i,yy}(x,y) \\ 0 & 0 & 0 & 2\mathfrak{X}_{i,xy}(x,y) \\ 0 & 0 & 0 & 0 \end{bmatrix}, \Upsilon_{b4}^i = \begin{bmatrix} 0 & 0 & 0 & 0 \\ 0 & 0 & 0 & 0 \\ 0 & 0 & 0 & 0 \\ 0 & 0 & 0 & \mathfrak{X}_i(x,y) \end{bmatrix}, \tag{21}$$

$$\Upsilon_{b5}^i = \begin{bmatrix} w_{b,x} + w_{s,x} & 0 \\ 0 & w_{b,y} + w_{s,y} \\ w_{b,y} + w_{s,y} & w_{b,x} + w_{s,x} \end{bmatrix}, \Upsilon_G^i = \begin{bmatrix} 0 & 0 & \mathfrak{X}_{i,x}(x,y) & \mathfrak{X}_{i,x}(x,y) \\ 0 & 0 & \mathfrak{X}_{i,y}(x,y) & \mathfrak{X}_{i,y}(x,y) \end{bmatrix}.$$

Therefore, strain tensor variations were derived as:

$$\begin{aligned} \delta(\mathfrak{F}_b) &= \delta(\mathfrak{F}_b^L) + \delta(\mathfrak{F}_b^{NL}) \\ &= \sum_{i=1}^{m\times n} \left( \Upsilon_{Lb}^i + \Upsilon_{NLb}^i \right) \begin{Bmatrix} \delta u^i \\ \delta v^i \\ \delta w_b^i \\ \delta w_s^i \end{Bmatrix}, \delta(\mathfrak{F}_s) \\ &= \sum_{i=1}^{m\times n} \Upsilon_s^i \begin{Bmatrix} \delta u^i \\ \delta v^i \\ \delta w_b^i \\ \delta w_s^i \end{Bmatrix}. \end{aligned} \tag{22}$$

In the continuation of solution methodology, the nonlinear differential equations of the system could be obtained in a discretized form as:

$$\mathfrak{A}(\mathbb{X})\mathbb{X} = \mathbb{S}, \tag{23}$$

where $\mathfrak{A}(\mathbb{X})$ is global stiffness matrix containing two nonlinear and linear parts as:

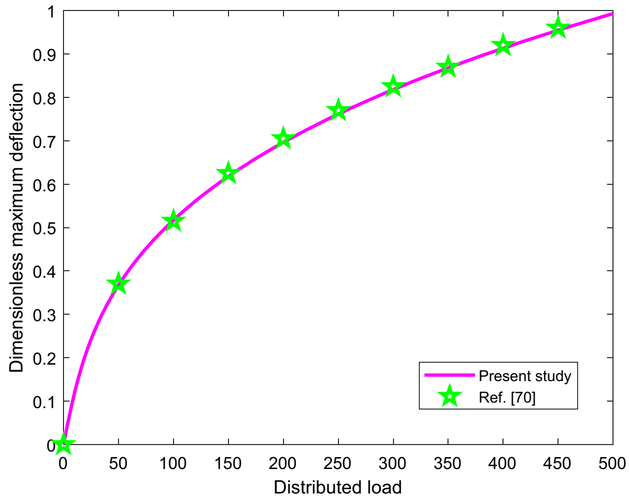


**Fig. 5** Comparison study on the load–deflection plots obtained for the nonlinear bending of a composite square plate under inform distributed load

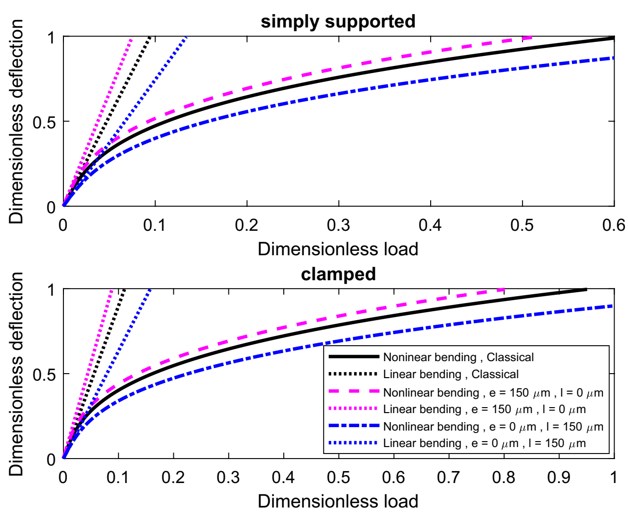


**Fig. 6** Comparison of the classical and nonlocal strain gradient plate models for linear and nonlinear flexural responses of FGM sector microplate with variable thickness ($k = 0.5, \eta = 1, \alpha = \pi/3$)

In addition, the load vector associated with uniform distributed load $\text{II}$ was stated as:

$$\mathbb{S} = \int_S \left(1 - e^2\nabla^2\right)\text{II}\begin{Bmatrix} 0 \\ 0 \\ \mathfrak{X}_i(x,y) \\ \mathfrak{X}_i(x,y) \end{Bmatrix} dS. \tag{26}$$

Then, an iterative procedure based on Newton–Raphson technique was applied to derive the solution of Eq. (23).

## 4 Numerical results and discussion

Following the application of the developed solution method, the dimensionless nonlocal strain gradient nonlinear and linear load–deflection behaviors of FGM microplates with a sector shape with variable thicknesses were drawn. It was assumed that FGM microplate bottom and top surfaces were fully metal and fully ceramic, respectively. Material properties were: $E_m = 70\,\text{GPa}$, $\nu = 0.35$ for metal constituent and $E_c = 210\,\text{GPa}$, $\nu = 0.24$ for ceramic constituent [69]. In addition, dimensionless maximum deflection was considered as $\underline{W}_{\max} = w_{\max}/h$ and dimensionless load was described as $P = \text{II}r_0^2/E_m h^2$. Furthermore, the geometric parameters of sector microplates with $h_0$ initial thickness were considered as $h_0 = 25\,\mu\text{m}$ and $2r_0 = 50h_0$.

Firstly, the proposed solving methodology was validated. To do so, neglecting couple stress size dependency terms, the nonlinear load–deflection curves drawn for geometrically nonlinear flexural behaviors of square composite plates were compared with those reported by Singh et al. [70], as shown in Fig. 5. A great agreement was witnessed which confirmed the reliability of the developed numerical solution process.

Figure 6 demonstrates dimensionless nonlocal strain gradient linear and nonlinear load–deflection responses corresponding to the flexural behavior of FGM sector microplates, with linear thickness variations ($\eta = 1$). To compare, the findings of classical quasi-3D continuum elasticity were also adopted. It was shown that increase of nonlocal parameter to plate thickness ratio enhanced nonlocality importance. However, decrease

$$\mathfrak{A}_L = \int_S \left\{ \left(\mathfrak{F}^i_{Lb}\right)^T \xi_b \mathfrak{F}^i_{Lb} - l^2\nabla^2\left(\mathfrak{F}^i_{Lb}\right)^T \xi_b \mathfrak{F}^i_{Lb} + \left(\mathfrak{F}^i_{s}\right)^T \xi_s \mathfrak{F}^i_{s} - l^2\nabla^2\left(\mathfrak{F}^i_{s}\right)^T \xi_s \mathfrak{F}^i_{s} \right\} dS, \tag{24}$$

$$\mathfrak{A}_{NL}(\mathbb{X}) = \int_S \left\{ \frac{1}{2}\left(\mathfrak{F}^i_{Lb}\right)^T \xi_b \mathfrak{F}^i_{NLb} - \frac{l^2}{2}\nabla^2\left(\mathfrak{F}^i_{Lb}\right)^T \xi_b \mathfrak{F}^i_{NLb} + \left(\mathfrak{F}^i_{NLb}\right)^T \xi_b \mathfrak{F}^i_{Lb} - l^2\nabla^2\left(\mathfrak{F}^i_{NLb}\right)^T \xi_b \mathfrak{F}^i_{Lb} + \frac{1}{2}\left(\mathfrak{F}^i_{NLb}\right)^T \xi_b \mathfrak{F}^i_{NLb} - \frac{l^2}{2}\nabla^2\left(\mathfrak{F}^i_{NLb}\right)^T \xi_b \mathfrak{F}^i_{NLb} \right\} dS. \tag{25}$$

**Table 1** Dimensionless classical and nonlocal strain gradient distributed loads associated with the nonlinear bending response of FGM sector microplates with simply supported boundary conditions corresponding to different nonlocal parameters and thickness variation constants

| $k$ | $e$ ($\mu$m) | $\eta = 0.3$ | $\eta = 0.6$ | $\eta = 1$ | $\eta = 1.3$ | $\eta = 1.6$ |
|---|---|---|---|---|---|---|
| $\alpha = \pi/3$ | | | | | | |
| 0.5 | $w/h = 0.4$ | | | | | |
| | 0 | 0.0671 | 0.0688 | 0.0713 | 0.0732 | 0.0759 |
| | 60 | 0.0651 (–2.90%) | 0.0667 (–2.89%) | 0.0693 (–2.88%) | 0.0711 (–2.87%) | 0.0738 (–2.86%) |
| | 120 | 0.0593 (–11.56%) | 0.0608 (–11.54%) | 0.0631 (–11.52%) | 0.0649 (–11.50%) | 0.0672 (–11.48%) |
| | $w/h = 0.8$ | | | | | |
| | 0 | 0.3290 | 0.3347 | 0.3434 | 0.3498 | 0.3587 |
| | 60 | 0.3203 (–2.63%) | 0.3260 (–2.62%) | 0.3344 (–2.61%) | 0.3407 (–2.60%) | 0.3494 (–2.59%) |
| | 120 | 0.2949 (–10.47%) | 0.2998 (–10.45%) | 0.3076 (–10.43%) | 0.3134 (–10.41%) | 0.3212 (–10.39%) |
| 2 | $w/h = 0.4$ | | | | | |
| | 0 | 0.0629 | 0.0645 | 0.0669 | 0.0687 | 0.0712 |
| | 60 | 0.0610 (–2.90%) | 0.0626 (–2.89%) | 0.0650 (–2.88%) | 0.0666 (–2.87%) | 0.0692 (–2.86%) |
| | 120 | 0.0556 (–11.56%) | 0.0570 (–11.54%) | 0.0592 (–11.52%) | 0.0609 (–11.50%) | 0.0630 (–11.48%) |
| | $w/h = 0.8$ | | | | | |
| | 0 | 0.3085 | 0.3139 | 0.3220 | 0.3281 | 0.3364 |
| | 60 | 0.3004 (–2.63%) | 0.3057 (–2.62%) | 0.3136 (–2.61%) | 0.3195 (–2.60%) | 0.3276 (–2.59%) |
| | 120 | 0.2763 (–10.47%) | 0.2811 (–10.45%) | 0.2884 (–10.43%) | 0.2939 (–10.41%) | 0.3013 (–10.39%) |
| $\alpha = \pi/2$ | | | | | | |
| 0.5 | $w/h = 0.4$ | | | | | |
| | 0 | 0.0493 | 0.0506 | 0.0532 | 0.0549 | 0.0569 |
| | 60 | 0.0485 (–1.62%) | 0.0497 (–1.61%) | 0.0523 (–1.60%) | 0.0541 (–1.59%) | 0.0559 (–1.58%) |
| | 120 | 0.0460 (–6.44%) | 0.0473 (–6.42%) | 0.0498 (–6.41%) | 0.0513 (–6.40%) | 0.0532 (–6.38%) |
| | $w/h = 0.8$ | | | | | |
| | 0 | 0.2428 | 0.2470 | 0.2560 | 0.2619 | 0.2684 |
| | 60 | 0.2393 (–1.46%) | 0.2434 (–1.46%) | 0.2523 (–1.45%) | 0.2581 (–1.44%) | 0.2645 (–1.43%) |
| | 120 | 0.2286 (–5.83%) | 0.2326 (–5.81%) | 0.2411 (–5.80%) | 0.2467 (–5.79%) | 0.2529 (–5.77%) |
| 2 | $w/h = 0.4$ | | | | | |
| | 0 | 0.0462 | 0.0474 | 0.0499 | 0.0515 | 0.0534 |
| | 60 | 0.0455 (–1.62%) | 0.0466 (–1.61%) | 0.0491 (–1.60%) | 0.0507 (–1.59%) | 0.0525 (–1.58%) |
| | 120 | 0.0434 (–6.44%) | 0.0443 (–6.42%) | 0.0467 (–6.41%) | 0.0482 (–6.40%) | 0.0501 (–6.38%) |
| | $w/h = 0.8$ | | | | | |
| | 0 | 0.2277 | 0.2316 | 0.2401 | 0.2456 | 0.2518 |
| | 60 | 0.2244 (–1.46%) | 0.2283 (–1.46%) | 0.2366 (–1.45%) | 0.2420 (–1.44%) | 0.2480 (–1.43%) |
| | 120 | 0.2143 (–5.83%) | 0.2182 (–5.81%) | 0.2261 (–5.80%) | 0.2313 (–5.79%) | 0.2372 (–5.77%) |

of the abovementioned ratio resulted in the tendency of both nonlinear and linear flexural behaviors of sector microplates to their classical counterparts. Similar findings were obtained for strain gradient size effect. Also, it was witnessed that considering nonlocal size effect resulted in higher extracted deflections obtained from nonlocal strain gradient quasi-3D plate model than those derived from classical continuum elasticity because of the softening property of nonlocal size effect, while strain gradient microstructural size dependency acted in opposite way and represented a stiffening property.

Tables 1 and 2 summarize the dimensionless distributed loads for specific values of maximum deflection in the presence of nonlocality and absence of strain gradient small scale effect for simply supported and clamped boundary conditions, respectively. The same findings are given in Tables 3 and 4 for strain gradient size effect and ignoring nonlocality, respectively. It was witnessed that by moving to deeper parts of load–deflection response, which takes into account higher maximum deflections, the significance of nonlocality softener character and strain gradient size dependency stiffer character somehow decreased. This finding was repeated for all thickness variation patterns and for both clamped and simply supported boundary conditions. However, it was found that changing material gradient index value changed

**Table 2** Dimensionless classical and nonlocal strain gradient distributed loads associated with the nonlinear bending response of FGM sector microplates with clamped boundary conditions corresponding to different nonlocal parameters and thickness variation constants

| $k$ | $e\,(\mu\mathrm{m})$ | $\eta = 0.3$ | $\eta = 0.6$ | $\eta = 1$ | $\eta = 1.3$ | $\eta = 1.6$ |
|---|---|---|---|---|---|---|
| $\alpha = \pi/3$ | | | | | | |
| 0.5 | $w/h = 0.4$ | | | | | |
| | 0 | 0.0958 | 0.0981 | 0.0989 | 0.1002 | 0.1034 |
| | 60 | 0.0931 (– 2.83%) | 0.0953 (– 2.82%) | 0.0961 (– 2.81%) | 0.0973 (– 2.80%) | 0.1006 (– 2.79%) |
| | 120 | 0.0850 (– 11.27%) | 0.0870 (– 11.25%) | 0.0878 (– 11.23%) | 0.0889 (– 11.21%) | 0.0919 (– 11.19%) |
| | $w/h = 0.8$ | | | | | |
| | 0 | 0.5127 | 0.5210 | 0.5242 | 0.5286 | 0.5410 |
| | 60 | 0.4994 (– 2.58%) | 0.5077 (– 2.57%) | 0.5108 (– 2.56%) | 0.5150 (– 2.55%) | 0.5271 (– 2.54%) |
| | 120 | 0.4601 (– 10.29%) | 0.4675 (– 10.27%) | 0.4705 (– 10.25%) | 0.4745 (– 10.23%) | 0.4855 (– 10.21%) |
| 2 | $w/h = 0.4$ | | | | | |
| | 0 | 0.0899 | 0.0920 | 0.0928 | 0.0939 | 0.0970 |
| | 60 | 0.0873 (– 2.83%) | 0.0894 (– 2.82%) | 0.0902 (– 2.81%) | 0.0912 (– 2.80%) | 0.0944 (– 2.79%) |
| | 120 | 0.0797 (– 11.27%) | 0.0815 (– 11.25%) | 0.0824 (– 11.23%) | 0.0834 (– 11.21%) | 0.0862 (– 11.19%) |
| | $w/h = 0.8$ | | | | | |
| | 0 | 0.4808 | 0.4886 | 0.4916 | 0.4957 | 0.5073 |
| | 60 | 0.4684 (– 2.58%) | 0.4761 (– 2.57%) | 0.4790 (– 2.56%) | 0.4830 (– 2.55%) | 0.4944 (– 2.54%) |
| | 120 | 0.4315 (– 10.29%) | 0.4385 (– 10.27%) | 0.4412 (– 10.25%) | 0.4450 (– 10.23%) | 0.4553 (– 10.21%) |
| $\alpha = \pi/2$ | | | | | | |
| 0.5 | $w/h = 0.4$ | | | | | |
| | 0 | 0.0710 | 0.0726 | 0.0737 | 0.0748 | 0.0778 |
| | 60 | 0.0698 (– 1.58%) | 0.0715 (– 1.57%) | 0.0726 (– 1.56%) | 0.0736 (– 1.55%) | 0.0767 (– 1.54%) |
| | 120 | 0.0664 (– 6.27%) | 0.0679 (– 6.25%) | 0.0691 (– 6.24%) | 0.0702 (– 6.23%) | 0.0730 (– 6.21%) |
| | $w/h = 0.8$ | | | | | |
| | 0 | 0.3805 | 0.3867 | 0.3908 | 0.3943 | 0.4059 |
| | 60 | 0.3751 (– 1.43%) | 0.3812 (– 1.42%) | 0.3852 (– 1.42%) | 0.3888 (– 1.42%) | 0.4001 (– 1.41%) |
| | 120 | 0.3588 (– 5.72%) | 0.3647 (– 5.70%) | 0.3685 (– 5.69%) | 0.3717 (– 5.68%) | 0.3827 (– 5.66%) |
| 2 | $w/h = 0.4$ | | | | | |
| | 0 | 0.0666 | 0.0681 | 0.0692 | 0.0700 | 0.0730 |
| | 60 | 0.0656 (– 1.58%) | 0.0671 (– 1.57%) | 0.0682 (– 1.56%) | 0.0690 (– 1.55%) | 0.0718 (– 1.54%) |
| | 120 | 0.0623 (– 6.27%) | 0.0639 (– 6.25%) | 0.0648 (– 6.24%) | 0.0656 (– 6.23%) | 0.0684 (– 6.21%) |
| | $w/h = 0.8$ | | | | | |
| | 0 | 0.3569 | 0.3627 | 0.3665 | 0.3698 | 0.3807 |
| | 60 | 0.3518 (– 1.43%) | 0.3574 (– 1.42%) | 0.3613 (– 1.42%) | 0.3646 (– 1.42%) | 0.3752 (– 1.41%) |
| | 120 | 0.3365 (– 5.72%) | 0.3419 (– 5.70%) | 0.3455 (– 5.69%) | 0.3487 (– 5.68%) | 0.3590 (– 5.66%) |

FGM sector microplate flexural stiffness, but the emphasis of both small scale effect kinds remained unchanged. This prediction was similar for both initial and deeper parts of flexural responses. Also, it was concluded that for all material gradient index values and thickness variation patterns, strain gradient size effect stiffer character was more prominent than nonlocality softener character acting in a specific value of maximum deflection.

Material gradient index effects on linear and nonlinear flexural responses of FGM sector microplates are presented in Fig. 7. Analyses were conducted for both classical and nonlocal strain gradient quasi-3D models. It was found that increase of material gradient index value, which resulted in moving from fully ceramic sector microplate to fully metal one, increased maximum deflection for a given uniform transverse load because of lower volume fractions of ceramic constituent. Also, it was found that in both nonlinear and linear flexural responses, increase of transverse load value enhanced the significance of material gradient index.

Figure 8 shows nonlocal strain gradient linear and flexural characteristics for FGM composite sector microplates with various thickness variation patterns. It was found that the gaps between load–deflection curves for concave, convex, and linear thickness variation patterns were increased by

**Table 3** Dimensionless classical and nonlocal strain gradient distributed loads associated with the nonlinear bending response of FGM sector microplates with simply supported boundary conditions corresponding to different strain gradient parameters and thickness variation constants

| $k$ | $l\,(\mu\text{m})$ | $\eta = 0.3$ | $\eta = 0.6$ | $\eta = 1$ | $\eta = 1.3$ | $\eta = 1.6$ |
|---|---|---|---|---|---|---|
| $\alpha = \pi/3$ | | | | | | |
| 0.5 | $w/h = 0.4$ | | | | | |
| | 0 | 0.0671 | 0.0688 | 0.0713 | 0.0732 | 0.0759 |
| | 60 | 0.0715 (+6.52%) | 0.0732 (+6.50%) | 0.0760 (+6.49%) | 0.0780 (+6.48%) | 0.0807 (+9.46%) |
| | 120 | 0.0847 (+26.01%) | 0.0867 (+25.98%) | 0.0898 (+25.96%) | 0.0922 (+25.94%) | 0.0954 (+25.91%) |
| | $w/h = 0.8$ | | | | | |
| | 0 | 0.3290 | 0.3347 | 0.3434 | 0.3498 | 0.3587 |
| | 60 | 0.3500 (+6.38%) | 0.3560 (+6.36%) | 0.3652 (+6.35%) | 0.3721 (+6.34%) | 0.3814 (+6.32%) |
| | 120 | 0.4126 (+25.42%) | 0.4197 (+25.39%) | 0.4305 (+25.37%) | 0.4385 (+25.35%) | 0.4496 (+25.32%) |
| 2 | $w/h = 0.4$ | | | | | |
| | 0 | 0.0629 | 0.0645 | 0.0669 | 0.0687 | 0.0712 |
| | 60 | 0.0671 (+6.52%) | 0.0687 (+6.50%) | 0.0712 (+6.49%) | 0.0732 (+6.48%) | 0.0757 (+6.46%) |
| | 120 | 0.0794 (+26.01%) | 0.0813 (+25.98%) | 0.0843 (+25.96%) | 0.0864 (+25.94%) | 0.0895 (+25.91%) |
| | $w/h = 0.8$ | | | | | |
| | 0 | 0.3085 | 0.3139 | 0.3220 | 0.3281 | 0.3364 |
| | 60 | 0.3282 (+6.38%) | 0.3338 (+6.36%) | 0.3425 (+6.35%) | 0.3489 (+6.34%) | 0.3576 (+6.32%) |
| | 120 | 0.3869 (+25.42%) | 0.3936 (+25.39%) | 0.4037 (+25.37%) | 0.4112 (+25.35%) | 0.4216 (+25.32%) |
| $\alpha = \pi/2$ | | | | | | |
| 0.5 | $w/h = 0.4$ | | | | | |
| | 0 | 0.0493 | 0.0506 | 0.0532 | 0.0549 | 0.0569 |
| | 60 | 0.0512 (+3.63%) | 0.0523 (+3.62%) | 0.0551 (+3.61%) | 0.0570 (+3.60%) | 0.0589 (+3.59%) |
| | 120 | 0.0565 (+14.47%) | 0.0578 (+14.45%) | 0.0608 (+14.44%) | 0.0629 (+14.43%) | 0.0650 (+14.41%) |
| | $w/h = 0.8$ | | | | | |
| | 0 | 0.2428 | 0.2470 | 0.2560 | 0.2619 | 0.2684 |
| | 60 | 0.2514 (+3.55%) | 0.2558 (+3.54%) | 0.2650 (+3.53%) | 0.2712 (+3.52%) | 0.2778 (+3.51%) |
| | 120 | 0.2771 (+14.14%) | 0.2818 (+14.12%) | 0.2921 (+14.11%) | 0.2989 (+14.10%) | 0.3063 (+14.08%) |
| 2 | $w/h = 0.4$ | | | | | |
| | 0 | 0.0462 | 0.0474 | 0.0499 | 0.0515 | 0.0534 |
| | 60 | 0.0479 (+3.63%) | 0.0491 (+3.62%) | 0.0517 (+3.61%) | 0.0535 (+3.60%) | 0.0553 (+3.59%) |
| | 120 | 0.0529 | 0.0542 | 0.0571 (+14.44%) | 0.0590 (+14.43%) | 0.0610 (+14.41%) |
| | $w/h = 0.8$ | | | | | |
| | 0 | 0.2277 | 0.2316 | 0.2401 | 0.2456 | 0.2518 |
| | 60 | 0.2357 (+3.55%) | 0.2399 (+3.54%) | 0.2485 (+3.53%) | 0.2543 (+3.52%) | 0.2607 (+3.51%) |
| | 120 | 0.2599 (+14.14%) | 0.2643 (+14.12%) | 0.2739 (+14.11%) | 0.2803 (+14.10%) | 0.2872 (+14.08%) |

altering the boundary conditions of FGM composite sector microplates from clamped to simply supported. In addition, it was found that at higher transverse loads, the effect of thickness variation pattern was enhanced.

Figure 9 shows the influences of geometrical parameters on nonlocal strain gradient linear and nonlinear flexural behaviors of FGM sector microplates. It was deduced that decrease of $\alpha$ in sector microplates increased their bending stiffness resulting in lower deflections for specific applied transverse loads. In addition, it was found that taking into account this variation in the geometrical parameter of sector microplates, the difference between nonlinear and linear flexural analyses was increased representing the increase of associated geometrical nonlinearity.

## 5 Concluding remarks

In this research, microstructural-dependent nonlinear and linear flexural properties of FGM microplates with a sector shape and different thicknesses were studied. To do so, nonlocal strain gradient continuum mechanics was applied

**Table 4** Dimensionless classical and nonlocal strain gradient distributed loads associated with the nonlinear bending response of FGM sector microplates with clamped boundary conditions corresponding to different strain gradient parameters and thickness variation constants

| $k$ | $l\,(\mu\text{m})$ | $\eta = 0.3$ | $\eta = 0.6$ | $\eta = 1$ | $\eta = 1.3$ | $\eta = 1.6$ |
|---|---|---|---|---|---|---|
| $\alpha = \pi/3$ | | | | | | |
| 0.5 | $w/h = 0.4$ | | | | | |
| | 0 | 0.0958 | 0.0981 | 0.0989 | 0.1002 | 0.1034 |
| | 60 | 0.1021 (+6.49%) | 0.1044 (+6.47%) | 0.1053 (+6.46%) | 0.1066 (+6.45%) | 0.1100 (+6.43%) |
| | 120 | 0.1208 (+25.86%) | 0.1235 (+25.83%) | 0.1245 (+25.81%) | 0.1258 (+25.79%) | 0.1300 (+25.76%) |
| | $w/h = 0.8$ | | | | | |
| | 0 | 0.5127 | 0.5210 | 0.5242 | 0.5286 | 0.5410 |
| | 60 | 0.5452 (+6.36%) | 0.5540 (+6.34%) | 0.5574 (+6.33%) | 0.5621 (+6.32%) | 0.5751 (+6.30%) |
| | 120 | 0.6424 (+25.33%) | 0.6528 (+25.30%) | 0.6567 (+25.28%) | 0.6621 (+25.26%) | 0.6776 (+25.23%) |
| 2 | $w/h = 0.4$ | | | | | |
| | 0 | 0.0899 | 0.0920 | 0.0928 | 0.0939 | 0.0970 |
| | 60 | 0.0958 (+6.49%) | 0.0979 (+6.47%) | 0.0988 (+6.46%) | 0.0999 (+6.45%) | 0.1032 (+6.43%) |
| | 120 | 0.1133 (+25.86%) | 0.1158 (+25.83%) | 0.1167 (+25.81%) | 0.1180 (+25.79%) | 0.1219 (+25.76%) |
| | $w/h = 0.8$ | | | | | |
| | 0 | 0.4808 | 0.4886 | 0.4916 | 0.4957 | 0.5073 |
| | 60 | 0.5113 (+6.36%) | 0.5196 (+6.34%) | 0.5228 (+6.33%) | 0.5271 (+6.32%) | 0.5394 (+6.30%) |
| | 120 | 0.6025 (+25.33%) | 0.6122 (+25.30%) | 0.6159 (+25.28%) | 0.6209 (+25.26%) | 0.6354 (+25.23%) |
| $\alpha = \pi/2$ | | | | | | |
| 0.5 | $w/h = 0.4$ | | | | | |
| | 0 | 0.0710 | 0.0726 | 0.0737 | 0.0748 | 0.0778 |
| | 60 | 0.0736 (+3.61%) | 0.0753 (+3.60%) | 0.0764 (+3.59%) | 0.0774 (+3.58%) | 0.0806 (+3.57%) |
| | 120 | 0.0813 (+14.38%) | 0.0831 (+14.36%) | 0.0843 (+14.35%) | 0.0854 (+14.34%) | 0.0890 (+14.32%) |
| | $w/h = 0.8$ | | | | | |
| | 0 | 0.3805 | 0.3867 | 0.3908 | 0.3943 | 0.4059 |
| | 60 | 0.3939 (+3.54%) | 0.4004 (+3.53%) | 0.4046 (+3.52%) | 0.4082 (+3.51%) | 0.4202 (+3.50%) |
| | 120 | 0.4341 (+14.09%) | 0.4411 (+14.07%) | 0.4458 (+14.06%) | 0.4498 (+14.05%) | 0.4629 (+14.03%) |
| 2 | $w/h = 0.4$ | | | | | |
| | 0 | 0.0666 | 0.0681 | 0.0692 | 0.0700 | 0.0730 |
| | 60 | 0.0691 (+3.61%) | 0.0706 (+3.60%) | 0.0716 (+3.59%) | 0.0726 (+3.58%) | 0.0756 (+3.57%) |
| | 120 | 0.0763 (+14.38%) | 0.0779 (+14.36%) | 0.0791 (+14.35%) | 0.0801 (+14.34%) | 0.0834 (+14.32%) |
| | $w/h = 0.8$ | | | | | |
| | 0 | 0.3569 | 0.3627 | 0.3665 | 0.3698 | 0.3807 |
| | 60 | 0.3695 (+3.54%) | 0.3755 (+3.53%) | 0.3794 (+3.52%) | 0.3829 (+3.51%) | 0.3941 (+3.50%) |
| | 120 | 0.4071 (+14.09%) | 0.4137 (+14.07%) | 0.4180 (+14.06%) | 0.4218 (+14.05%) | 0.4341 (+14.03%) |

in a hybrid quasi-3D-based higher order shear deformation plate model along with von Karman geometrical nonlinearity. Then, isogeometric finite element method was applied to derive nonlocal strain gradient nonlinear and linear load–deflection plots along with classical continuum elastic-based counterparts.

It was shown that by moving to deeper parts of load–deflection responses which took into account higher maximum deflections, the significance of strain gradient size dependency stiffer character and nonlocality softener character was somehow decreased. Furthermore, for all thickness variation patterns and material gradient index values, strain gradient size effect stiffer character was more prominent than nonlocality softener character acting in a specific value of maximum deflection. This anticipation was similar for both initial and deeper parts of flexural responses. Furthermore, it was found that at higher applied transverse loads, the importance of thickness variation pattern effect was enhanced.

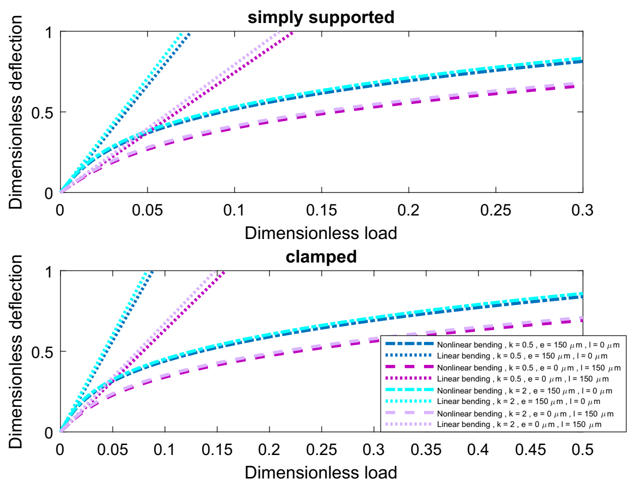


**Fig. 7** Influence of material gradient index on the nonlocal strain gradient linear and nonlinear flexural responses of FGM sector microplate with variable thickness ($\eta = 1, \alpha = \pi/3$)

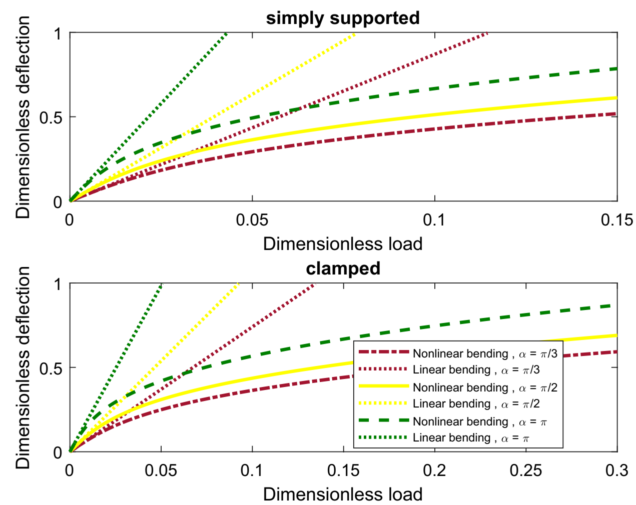


**Fig. 9** Influence of the angle on the nonlocal strain gradient linear and nonlinear flexural responses of FGM sector microplate with variable thickness ($k = 0.5, \eta = 1, e = l = 150\ \mu$m)

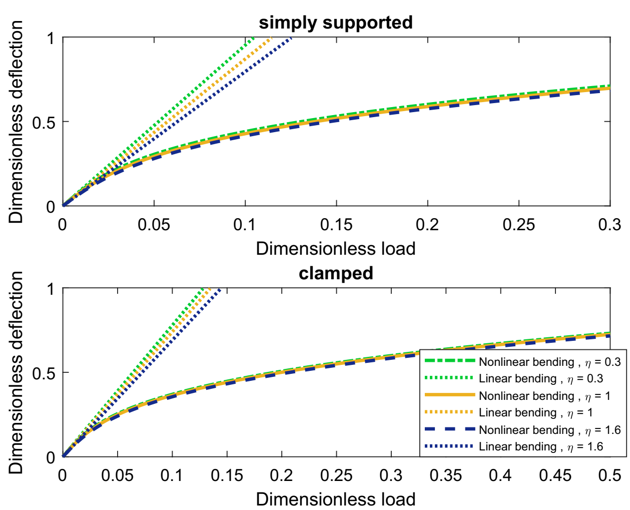


**Fig. 8** Influence of thickness variation parameter on the nonlocal strain gradient linear and nonlinear flexural responses of FGM sector microplate with variable thickness ($k = 0.5, e = l = 150\ \mu$m, $\alpha = \pi/3$ )

## References


1. Kumar S, Murthy Reddy KVVS, Kumar A, Rohini Devi G (2013) Development and characterization of polymer–ceramic continuous fiber reinforced functionally graded composites for aerospace application. Aerosp Sci Technol 26:185–191
2. Gao WL, Qin ZY, Chu FL (2020) Wave propagation in functionally graded porous plates reinforced with graphene platelets. Aerosp Sci Technol 102:105860
3. Liu YF, Qin ZY, Chu FL (2020) Analytical study of the impact response of shear deformable sandwich cylindrical shell with a functionally graded porous core. Mech Adv Mater Struct. https://doi.org/10.1080/15376494.2020.1818904
4. Qin ZY, Chu FL, Zu J (2017) Free vibrations of cylindrical shells with arbitrary boundary conditions: a comparison study. Int J Mech Sci 133:91–99
5. Qin ZY, Yang ZB, Zu J, Chu FL (2018) Free vibration analysis of rotating cylindrical shells coupled with moderately thick annular plate. Int J Mech Sci 142:127–139
6. Li H, Lv HY, Sun H, Qin ZY, Xiong J, Han QK, Liu JG, Wang XP (2021) Nonlinear vibrations of fiber-reinforced composite cylindrical shells with bolt loosening boundary conditions. J Sound Vib 496(31):115935
7. Zuo C, Chen Q, Gu G, Feng S, Feng F et al (2013) High-speed three-dimensional shape measurement for dynamic scenes using hi-frequency tripolar pulse-width-modulation fringe projection. Opt Lasers Eng 51:953–960
8. Mou B, Bai Y (2018) Experimental investigation on shear behavior of steel beam-to-CFST column connections with irregular panel zone. Eng Struct 168:487–504
9. Mou B, Li X, Bai Y, Wang L (2019) Shear behavior of panel zones in steel beam-to-column connections with unequal depth of outer annular stiffener. J Struct Eng 145:1943
10. Mou B, Zhao F, Qiao Q, Wang L, Li H et al (2019) Flexural behavior of beam to column joints with or without an overlying concrete slab. Eng Struct 199:109616
11. Gholipour G, Zhang C, Mousavi AA (2020) Numerical analysis of axially loaded RC columns subjected to the combination of impact and blast loads. Eng Struct 219:110924
12. Abedini M, Zhang C (2021) Blast performance of concrete columns retrofitted with FRP using segment pressure technique. Compos Struct 260:113473
13. Wang J, Lu S, Wang Y, Li C, Wang K (2020) Effect analysis on thermal behavior enhancement of lithium–ion battery pack with different cooling structures. J Energy Storage 32:101800
14. Zhang J, Sun J, Chen Q, Zuo C (2020) Resolution analysis in a lens-free on-chip digital holographic microscope. IEEE Trans Comput Imaging 6:697–710
15. Hu Y, Chen Q, Feng S, Zuo C (2020) Microscopic fringe projection profilometry: a review. Opt Lasers Eng 135:106192
16. Zheng J, Zhang C, Li A (2020) Experimental investigation on the mechanical properties of curved metallic plate dampers. Appl Sci 10:269

17. Jung W-Y, Han S-C (2015) Static and eigenvalue problems of Sigmoid Functionally Graded Materials (S-FGM) micro-scale plates using the modified couple stress theory. Appl Math Model 39:3506–3524
18. Li YS, Pan E (2015) Static bending and free vibration of a functionally graded piezoelectric microplate based on the modified couple-stress theory. Int J Eng Sci 97:40–59
19. Simsek M (2016) Nonlinear free vibration of a functionally graded nanobeam using nonlocal strain gradient theory and a novel Hamiltonian approach. Int J Eng Sci 105:12–27
20. Sahmani S, Aghdam MM (2017) Imperfection sensitivity of the size-dependent postbuckling response of pressurized FGM nanoshells in thermal environments. Arch Civ Mech Eng 17:623–638
21. Liu JC, Zhang YQ, Fan LF (2017) Nonlocal vibration and biaxial buckling of double-viscoelastic-FGM-nanoplate system with viscoelastic Pasternak medium in between. Phys Lett A 381:1228–1235
22. Sahmani S, Aghdam MM (2017) Nonlinear instability of hydrostatic pressurized hybrid FGM exponential shear deformable nanoshells based on nonlocal continuum elasticity. Compos B Eng 114:404–417
23. Sahmani S, Aghdam MM (2017) Temperature-dependent nonlocal instability of hybrid FGM exponential shear deformable nanoshells including imperfection sensitivity. Int J Mech Sci 122:129–142
24. Sahmani S, Aghdam MM (2017) Size dependency in axial postbuckling behavior of hybrid FGM exponential shear deformable nanoshells based on the nonlocal elasticity theory. Compos Struct 166:104–113
25. Phung-Van P, Tran LV, Ferreira AJM, Nguyen-Xuan H, Abdel-Wahab M (2017) Nonlinear transient isogeometric analysis of smart piezoelectric functionally graded material plates based on generalized shear deformation theory under thermo-electro-mechanical loads. Nonlinear Dyn 87:879–894
26. Nguyen HX, Nguyen TN, Abdel-Wahab M, Bordas SPA, Nguyen-Xuan H, Vo TP (2017) A refined quasi-3D isogeometric analysis for functionally graded microplates based on the modified couple stress theory. Comput Methods Appl Mech Eng 313:904–940
27. Phung-Van P, Ferreira AJM, Nguyen-Xuan H, Abdel Wahab M (2017) An isogeometric approach for size-dependent geometrically nonlinear transient analysis of functionally graded nanoplates. Compos Part B Eng 118:125–134
28. Chu L, Dui G, Ju C (2018) Flexoelectric effect on the bending and vibration responses of functionally graded piezoelectric nanobeams based on general modified strain gradient theory. Compos Struct 186:39–49
29. Khakalo S, Balobanov V, Niiranen J (2018) Modelling size-dependent bending, buckling and vibrations of 2D triangular lattices by strain gradient elasticity models: applications to sandwich beams and auxetics. Int J Eng Sci 127:33–52
30. She G-L, Yuan F-G, Ren Y-R, Liu H-B, Xiao W-S (2018) Nonlinear bending and vibration analysis of functionally graded porous tubes via a nonlocal strain gradient theory. Compos Struct 203:614–623
31. Pang M, Li ZL, Zhang YQ (2018) Size-dependent transverse vibration of viscoelastic nanoplates including high-order surface stress effect. Phys B 545:94–98
32. Sahmani S, Aghdam MM, Rabczuk T (2018) Nonlinear bending of functionally graded porous micro/nano-beams reinforced with graphene platelets based upon nonlocal strain gradient theory. Compos Struct 186:68–78
33. Sahmani S, Aghdam MM, Rabczuk T (2018) A unified nonlocal strain gradient plate model for nonlinear axial instability of functionally graded porous micro/nano-plates reinforced with graphene platelets. Mater Res Express 5:045048
34. Sahmani S, Aghdam MM, Rabczuk T (2018) Nonlocal strain gradient plate model for nonlinear large-amplitude vibrations of functionally graded porous micro/nano-plates reinforced with GPLs. Compos Struct 198:51–62
35. Sahmani S, Aghdam MM (2017) Axial postbuckling analysis of multilayer functionally graded composite nanoplates reinforced with GPLs based on nonlocal strain gradient theory. Eur Phys J Plus 132:1–17
36. Phung-Van P, Thai CH, Nguyen-Xuan H, Abdel Wahab M (2019) Porosity-dependent nonlinear transient responses of functionally graded nanoplates using isogeometric analysis. Compos Part B Eng 164:215–225
37. Li Q, Wu D, Gao W, Tin-Loi F, Liu Z, Cheng J (2019) Static bending and free vibration of organic solar cell resting on Winkler-Pasternak elastic foundation through the modified strain gradient theory. Eur J Mech A Solids 78:103852
38. Thanh C-L, Tran LV, Vu-Huu T, Abdel-Wahab M (2019) The size-dependent thermal bending and buckling analyses of composite laminate microplate based on new modified couple stress theory and isogeometric analysis. Comput Methods Appl Mech Eng 350:337–361
39. Sahmani S, Safaei B (2019) Nonlinear free vibrations of bi-directional functionally graded micro/nano-beams including nonlocal stress and microstructural strain gradient size effects. Thin Walled Struct 140:342–356
40. Sahmani S, Safaei B (2019) Nonlocal strain gradient nonlinear resonance of bi-directional functionally graded composite micro/nano-beams under periodic soft excitation. Thin Walled Struct 143:106226
41. Sahmani S, Safaei B (2020) Influence of homogenization models on size-dependent nonlinear bending and postbuckling of bi-directional functionally graded micro/nano-beams. Appl Math Model 82:336–358
42. Fan F, Xu Y, Sahmani S, Safaei B (2020) Modified couple stress-based geometrically nonlinear oscillations of porous functionally graded microplates using NURBS-based isogeometric approach. Comput Methods Appl Mech Eng 372:113400
43. Fan F, Lei B, Sahmani S, Safaei B (2020) On the surface elastic-based shear buckling characteristics of functionally graded composite skew nanoplates. Thin Walled Struct 154:106841
44. Fan F, Safaei B, Sahmani S (2021) Buckling and postbuckling response of nonlocal strain gradient porous functionally graded micro/nano-plates via NURBS-based isogeometric analysis. Thin Walled Struct 159:107231
45. Ghorbani K, Mohammadi K, Rajabpour A, Ghadiri M (2019) Surface and size-dependent effects on the free vibration analysis of cylindrical shell based on Gurtin-Murdoch and nonlocal strain gradient theories. J Phys Chem Solids 129:140–150
46. Yuan Y, Zhao K, Zhao Y, Sahmani S, Safaei B (2020) Couple stress-based nonlinear buckling analysis of hydrostatic pressurized functionally graded composite conical microshells. Mech Mater 148:103507
47. Yuan Y, Zhao K, Han Y, Sahmani S, Safaei B (2020) Nonlinear oscillations of composite conical microshells with in-plane heterogeneity based upon a couple stress-based shell model. Thin Walled Struct 154:106857
48. Yuan Y, Zhao X, Zhao Y, Sahmani S, Safaei B (2021) Dynamic stability of nonlocal strain gradient FGM truncated conical microshells integrated with magnetostrictive facesheets resting on a nonlinear viscoelastic foundation. Thin Walled Struct 159:107249
49. Ghobadi A, Golestanian H, Tadi Beni Y, Kamil Zur K (2021) On the size-dependent nonlinear thermo-electro-mechanical free vibration analysis of functionally graded flexoelectric nano-plate. Commun Nonlinear Sci Numer Simul 95:105585

50. Thai CH, Tran TD, Phung-Van P (2020) A size-dependent moving Kriging meshfree model for deformation and free vibration analysis of functionally graded carbon nanotube-reinforced composite nanoplates. Eng Anal Bound Elem 115:52–63
51. Yuan Y, Zhao K, Sahmani S, Safaei B (2020) Size-dependent shear buckling response of FGM skew nanoplates modeled via different homogenization schemes. Appl Math Mech 41:587–604
52. Yi H, Sahmani S, Safaei B (2020) On size-dependent large-amplitude free oscillations of FGPM nanoshells incorporating vibrational mode interactions. Arch Civ Mech Eng 20:1–23
53. Li Q, Xie B, Sahmani S, Safaei B (2020) Surface stress effect on the nonlinear free vibrations of functionally graded composite nanoshells in the presence of modal interaction. J Braz Soc Mech Sci Eng 42:237
54. Fan L, Sahmani S, Safaei B (2021) Couple stress-based dynamic stability analysis of functionally graded composite truncated conical microshells with magnetostrictive facesheets embedded within nonlinear viscoelastic foundations. Eng Comput 37:1635–1655
55. Sarafraz A, Sahmani S, Aghdam MM (2019) Nonlinear secondary resonance of nanobeams under subharmonic and superharmonic excitations including surface free energy effects. Appl Math Model 66:195–226
56. Xie B, Sahmani S, Safaei B, Xu B (2021) Nonlinear secondary resonance of FG porous silicon nanobeams under periodic hard excitations based on surface elasticity theory. Eng Comput 37:1611–1634
57. Yang X, Sahmani S, Safaei B (2021) Postbuckling analysis of hydrostatic pressurized FGM microsized shells including strain gradient and stress-driven nonlocal effects. Eng Comput 37:1549–1564
58. Yang F, Chong ACM, Lam DCC et al (2002) Couple stress based strain gradient theory for elasticity. Int J Solids Struct 39:2731–2743
59. Eringen AC (1982) On differential equations of nonlocal elasticity and solutions of screw dislocation and surface waves. J Appl Phys 54:4703–4710
60. Thai CH, Ferreira AJM, Phung-Van P (2020) A nonlocal strain gradient isogeometric model for free vibration and bending analyses of functionally graded plates. Compos Struct 251:112634
61. Van Do VN, Lee C-H (2020) Bézier extraction based isogeometric analysis for bending and free vibration behavior of multilayered functionally graded composite cylindrical panels reinforced with graphene platelets. Int J Mech Sci 183:105744
62. Bekhoucha F (2021) Isogeometric analysis for in-plane free vibration of centrifugally stiffened beams including Coriolis effects. Mech Res Commun 111:103645
63. Yin S, Deng Y, Yu T, Gu S, Zhang G (2021) Isogeometric analysis for non-classical Bernoulli-Euler beam model incorporating microstructure and surface energy effects. Appl Math Model 89:470–485
64. Fan F, Sahmani S, Safaei B (2021) Isogeometric nonlinear oscillations of nonlocal strain gradient PFGM micro/nano-plates via NURBS-based formulation. Compos Struct 255:112969
65. Fan F, Cai X, Sahmani S, Safaei B (2021) Isogeometric thermal postbuckling analysis of porous FGM quasi-3D nanoplates having cutouts with different shapes based upon surface stress elasticity. Compos Struct 262:113604
66. Chen SX, Sahmani S, Safaei B (2021) Size-dependent nonlinear bending behavior of porous FGM quasi-3D microplates with a central cutout based on nonlocal strain gradient isogeometric finite element modelling. Eng Comput 37:1657–1678
67. Qiu J, Sahmani S, Safaei B (2020) On the NURBS-based isogeometric analysis for couple stress-based nonlinear instability of PFGM microplates. Mech Based Des Mach Struct. https://doi.org/10.1080/15397734.2020.1853567
68. Tao C, Dai T (2021) Isogeometric analysis for size-dependent nonlinear free vibration of graphene platelet reinforced laminated annular sector microplates. Eur J Mech A Solids 86:104171
69. Miller RE, Shenoy VB (2000) Size-dependent elastic properties of nanosized structural elements. Nanotechnology 11:139–147
70. Singh G, Rao GV, Iyengar NGR (1994) Geometrically nonlinear flexural response characteristics of shear deformable unsymmetrically laminated plates. Comput Struct 53:69–81